A Direct Evaluation of Stress Intensity Factors Using the Extended Dual Boundary Element Method

I.A. Alatawi and J. Trevelyan

Abstract

We introduce an alternative method in computational fracture mechanics to evaluate Stress Intensity Factors (SIFs) directly using the Extended Dual Boundary Element Method (XBEM) for 2D problems. Like other enrichment approaches, the new approach is able to yield accurate results on coarse discretisations, and the enrichment increases the problem size by only two degrees of freedom per crack tip. The BEM equations formed by collocation at nodes are augmented by two additional equations that enforce continuity of displacement at the crack tip. The enrichment approach provides the values of SIFs K_I and K_{II} directly in the solution vector and without any need for postprocessing such as the J-integral. Numerical examples are used to compare the accuracy of these directly computed SIFs to J-integral processing of both conventional and enriched boundary element approximations.

1   Introduction

In making fracture assessments, and in particular the prediction of crack propagation, it is of great importance to have an accurate understanding of the stress field in the vicinity of the crack tip. In Linear Elastic Fracture Mechanics (LEFM), the Stress Intensity Factors (SIFs) play a major role in the description of the the singular stress field, and can be seen in the stress and displacement expansions introduced by Williams [1]. SIFs can be determined from handbooks (e.g. [2]) for some simple cases of geometry and loading. For complicated shapes or applied boundary conditions, engineers can make use of numerical methods to resolve the stress fields and thereby give the SIFs K_I and K_{II} for modes I and II, respectively. It is well known that a singularity appears at the crack tip in LEFM, making numerical methods such as Finite Element Method (FEM) and Boundary Element Method (BEM) inefficient without modification. Watwood [3] noted the need for using a very refined mesh near the crack tip. Much of the computational fracture mechanics research work since then has involved developing algorithms that, in one way or another, offer a more efficient solution. In an early example of enriched FEM formulations, Benzley [4] successfully determined SIFs using isoparametric finite elements enriched locally with functions to

capture point singularities. Henshell and Shaw [5] presented the use of quarter-point elements, in which the desired $\sqrt{r}$ (where r is the distance from the crack tip) variation in displacements could be achieved by moving the mid-nodes of elements to quarter-point positions.

Contributions to computational fracture mechanics continued with the hybrid crack element introduced by Tong et al. [6] and extended by Xiao and Karihaloo [7], showing how it can be used for direct evaluation of singular and higher order coefficients. In parallel, Leung and Su [8, 9] introduced the fractal finite element method which divides the domain into a regular and a singular region, where the crack tip is the centre of similarity of the singular region. The method was applied to modes I, II and III successfully and has shown an accuracy of (1%) [10]. Recently, extensions of the method have been added including fractal hybrid finite elements [11] and fractal-like FEM [12] for bi-material problems. The Scaled Boundary Finite Element Method (SBFEM) [13] benefits from its semianalytical formulation to provide highly accurate approximations for the SIFs. The method suffers from its restriction to star-shaped domains (i.e. those exhibiting a line-of-sight to all boundary points from the "scaling centre" which is placed at the crack tip in fracture problems) or models comprising a set of star-shaped subdomains. This restriction has been overcome by coupling the SBFEM to the BEM [14].

The partition of unity method was introduced as a general technique to allow enrichment of FEM approximations. Melenk & Babuška [15] showed how the traditional piecewise polynomial approximation basis can be enriched by the use of functions (or sets of functions) that offer better approximation properties. This idea has been applied to computational fracture mechanics in the form of the Extended Finite Element Method (XFEM) [16]. The use of XFEM enrichment led to a reduction in the need for mesh refinement, and also separated the mesh from the crack path so crack propagation analysis could proceed with the need for remeshing, and for these reasons it has spawned a considerable volume of literature.

In parallel with the development of finite element methods, the Boundary Element Method (BEM) also gained popularity because of its boundary-only meshing (offering a reduction in dimensionality of the problem) and because of its ability to capture discontinuous functions. It also offered good accuracy of solutions on the domain boundary whereas finite element methods offered their greatest accuracy at integration points within the element. However, using the classical BEM to collocate on coincident points on opposing crack surfaces gives rise to degenerate linear systems [17]. Many methods have been proposed offering various treatments including special Green's functions [18] and the subregion technique [19]. Hong and Chen [20, 21] introduced the idea of Dual Boundary Integral Equations, in which a combination of the standard Boundary Integral Equation and its derivative can be used to provide independent equations in order to overcome the problem of degeneracy. They showed how the Displacement Boundary Integral Equation (DBIE) can be differentiated and Hookes law applied to derive the Traction Boundary Integral Equation (TBIE). Chen and Hong [22] for the first time solved a system formed from a combination of the

two integral equations in the context of a Darcy problem, but Portela et al. [23] were the rst to implement the combined use of the DBIE and TBIE in a single system to solve crack problems. They named this the Dual Boundary Element Method. Hong and Chen [24] reviewed the Dual BEM development up to the end of the 1990s. Portela et al [23] also described how the use of the TBIE imposes certain conditions on the selection of elements used for the discretisation of crack surfaces. These conditions arise because of the continuity requirements of the field variables for the existence of Cauchy and Hadamard principal value integrals. It is routine to overcome the problem while still using collocation by using discontinuous elements, in which the nodes are located within the body of the element, and not at its ends. Collocation at these nodes satisfies the Holder continuity requirements of the hypersingular integral equation since the shape functions are continuously differentiable at these points. There is considerable literature describing the application of discontinuous element for this purpose e.g. [23, 25, 26, 27]. These elements also permit the analysis of wide variety of crack geometries including kinked cracks.

The use of the Williams expansions in the BEM has been presented by Portela et al. [28] to subtract the singularity by dividing the domain into singular and regular fields. The technique was able to solve for K_I and K_{II} directly. Recently, the partition of unity approach was used by Simpson and Trevelyan [29], who presented a boundary element method enriched in a similar fashion to XFEM (giving a technique that could be called XBEM, as we continue to call it henceforth). This work extended the benefits of XFEM to provide high accuracy of SIFs from coarse boundary-only discretisations. Their method was soon extended to curved cracks [30]. Both implementations relied on the use of the J-integral [31] to calculate the SIFs. In the current paper, we extend this XBEM approach by using a modified form of enrichment in combination with crack tip displacement constraint equations to provide values of SIFs directly. The aim is to enable the solution of large problems, particularly when the enrichment is extended to 3D, by making a considerable reduction in the number of degrees of freedom required to achieve results of a prescribed accuracy. We note that other approaches to acceleration of BEM simulations have been developed, e.g. the Fast Multipole Method (FMM), which has been applied successfully to speed up the evaluation for thousands of cracks [32]. The authors believe the enriched XBEM approach described in this article could be further accelerated with the FMM to provide a powerful solution. Unlike [32] the proposed method is able to evaluate SIFs directly at a cost of two additional degrees of freedom per crack tip. This is an interesting subject for further research.

A similar square root enrichment was earlier introduced into the shape functions for special crack tip elements by Li et al. [33], and applied to the relative crack face displacements in a symmetric Galerkin BEM based on weak form integral equations. Like [29, 30] this technique was shown to give good accuracy from coarse meshes. The approach of [29, 30] is adopted in the current work as it offers similar accuracy benefits but can be more easily implemented by making a relatively simple modification to a pre-existing DBEM code.

In general determination of SIFs can be categorized into direct and post-

processing methods. Direct methods offer speed and flexibility to evaluate higher order terms [7]. On the other hand, the J-integral, taken over a closed independent integral path and based on energy approach, is the most used post-processing technique and is available to general purpose FEM and BEM codes that do not have any special formulations injected to deal directly with the stress singularity.

In this paper, we introduce a direct, highly accurate evaluation of SIFs by enriching crack surface elements. Moreover, it has potential for extension to 3D, where the use of the J-integral type approaches become more cumbersome than in 2D.

2 Extended (Dual) Boundary Element Method

Applying the classical direct collocation BEM to problems containing cracks leads to rank deficiency since duplicate equations are formed when collocating at coincident nodes on opposing crack surfaces. The Dual Boundary Element Method (DBEM) [23] overcomes this difficulty and is an efficient technique for modelling crack problems in BEM. The method consists of two independent boundary integral equations; where the Displacement Boundary Integral Equation (DBIE) is used when collocating on one crack surface, and the Traction Boundary Integral Equation (TBIE) is used on the another surface. Moreover, discontinuous elements are used for the geometry discretisations to meet continuity requirement as shown in Fig. 1. The DBIE used on the upper surface is given by

$$C_{ij}(\grave{x})u_j(\grave{x}) + C_{ij}(\hat{x})u_j(\hat{x}) + \int_\Gamma T_{ij}(\grave{x},x)u_j(x)d\Gamma = \int_\Gamma U_{ij}(\grave{x},x)t_j(x)d\Gamma, \quad (1)$$

where T_{ij} and U_{ij} are the traction and displacement fundamental solutions, and $C_{ij}u_j$ represents a jump term that emerges as a result of the strongly singular integral of the traction kernel. x and $\grave{x}$ denote the usual field point and source point in boundary element methods, and $\hat{x}$ is the point coincident with the source $\grave{x}$ but lying on the opposing crack surface as shown in Figure 1. The TBIE can be obtained by differentiating the DBIE in the k direction with respect to the normal direction at source point $\grave{x}$, and can be written for a smooth boundary as follows,

$$\frac{1}{2}t_j(\grave{x}) - \frac{1}{2}t_j(\hat{x}) + n_i(\grave{x})\int_\Gamma S_{kij}(\grave{x},x)u_k(x)d\Gamma = n_i(\grave{x})\int_\Gamma D_{kij}(\grave{x},x)t_k(x)d\Gamma, \quad (2)$$

where S_{kij} and D_{kij} are derivative kernels obtained by differentiating the fundamental solution. In this paper we consider traction-free cracks, so that $t_j(\grave{x})$ and $t_j(\hat{x})$ in (2) vanish, and will be dropped in the description of the enriched form of the TBIE.

2.1 Extended boundary integral equation formulation

The stress singularity at the crack tip cannot be captured by standard quadratic interpolation of displacements in the BEM unless highly refined meshes are used. As an alternative, the extended boundary element method introduced by Simpson and Trevelyan [29] shows an improvement of accuracy using coarse meshes, made possible by the use of the asymptotic, analytical expression for displacements around the crack tip within the BIE. The well-known Williams expansion for displacements near the crack tip can be written as

$$u_j = K_I \psi_{Ij}(r, \theta) + K_{II} \psi_{IIj}(r, \theta) \tag{3}$$

where K_I and K_{II} are the mode I and mode II stress intensity factors, and the terms $\psi_{Ij}(r, \theta)$ and $\psi_{IIj}(r, \theta)$ are given by the following functions:

$$\psi_{Ix} = \frac{1}{2\mu} \sqrt{\frac{r}{2\pi}} \cos \frac{\theta}{2} \left[\kappa - 1 + 2 \sin^2 \frac{\theta}{2} \right] \tag{4a}$$

$$\psi_{IIx} = \frac{1}{2\mu} \sqrt{\frac{r}{2\pi}} \sin \frac{\theta}{2} \left[\kappa + 1 + 2 \cos^2 \frac{\theta}{2} \right] \tag{4b}$$

$$\psi_{Iy} = \frac{1}{2\mu} \sqrt{\frac{r}{2\pi}} \sin \frac{\theta}{2} \left[\kappa + 1 - 2 \cos^2 \frac{\theta}{2} \right] \tag{4c}$$

$$\psi_{IIy} = \frac{-1}{2\mu} \sqrt{\frac{r}{2\pi}} \cos \frac{\theta}{2} \left[\kappa - 1 - 2 \sin^2 \frac{\theta}{2} \right] \tag{4d}$$

where r and θ are polar coordinates centered at the crack tip, μ is the shear modulus and κ is a parameter defined as $\kappa = 3 - 4v$ and $\kappa = \frac{3-v}{1+v}$ for plane strain and plane stress, respectively, v being the Poisson's ratio. Equation (3) can be used to enrich an otherwise classical piecewise polynomial shape function approximation of displacement near the crack tip, in a fashion similar to the early work of Benzley [4], as follows,

$$u_j = \tilde{K}_I \psi_{Ij} + \tilde{K}_{II} \psi_{IIj} + \sum_{a=1}^{M} N^a u_j^a \tag{5}$$
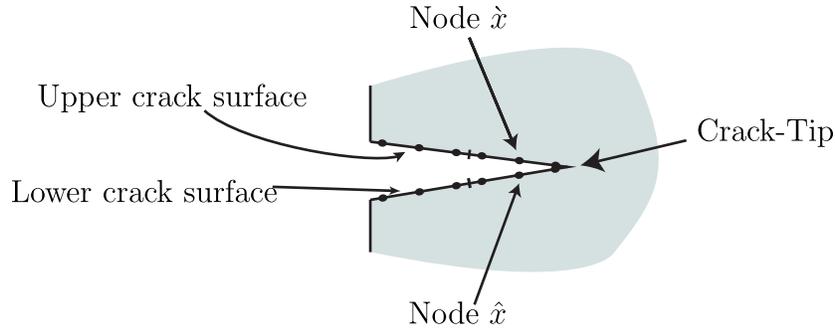
Figure 1: Crack characteristics with DBEM

where u_j^a is no longer the nodal displacement (as in the conventional BEM), but is instead to be viewed simply as a coefficient scaling the Lagrangian shape function N^a for node a, and M is the total number of element nodes. Equation (3) is able to approximate well the displacement near the crack tip. It is noted that (3) predicts the displacement components to vanish at the crack tip, i.e. at $r = 0$. Therefore an important role of the last term in (5) is to capture a non-zero displacement of the crack tip. The coefficients $\tilde{K}_I$ and $\tilde{K}_{II}$ are the unknown amplitudes of the enrichment functions ψ_{Ij}, ψ_{IIj} and are found as terms in the XBEM solution vector. When this enriched form of the displacement is used, the DBIE (1) can be written in a discretised form,

$$C_{ij}(\dot{x})u_j(\dot{x}) + C_{ij}(\hat{x})u_j(\hat{x}) + \sum_{n=1}^{Ne}\sum_{a=1}^{M} P_{ij}^{na}u_j^{na} + \sum_{a=1}^{Ne} \tilde{P}_{ijI}^n \tilde{K}_I$$
$$+ \sum_{a=1}^{Ne} \tilde{P}_{ijII}^n \tilde{K}_{II} = \sum_{n=1}^{Ne}\sum_{a=1}^{M} Q_{ij}^{na}t_j^{na} \tag{6}$$

where

$$P_{ij}^{na} = \int_{-1}^{1} N^a(\xi)T_{ij}(\dot{x}, x(\xi))J^n(\xi)d\xi \tag{7a}$$

$$Q_{ij}^{na} = \int_{-1}^{1} N^a(\xi)U_{ij}(\dot{x}, x(\xi))J^n(\xi)d\xi \tag{7b}$$

$$\tilde{P}_{ijI}^n = \int_{-1}^{1} T_{ij}(\dot{x}, x(\xi))\psi_{Ij}(\xi)J^n(\xi)d\xi \tag{7c}$$

$$\tilde{P}_{ijII}^n = \int_{-1}^{1} T_{ij}(\dot{x}, x(\xi))\psi_{IIj}(\xi)J^n(\xi)d\xi \tag{7d}$$

Ne and M are the total number of elements and the number of nodes per element, respectively, $\xi \in (-1, 1)$ is the local parametric coordinate used to describe the element, and $J^n(\xi)$ is the Jacobian of coordinate transformation.

We enrich only elements on the crack surfaces and in the vicinity of the crack tips, so that for most elements the displacement is expressed in the usual shape function form. If element n is unenriched then $\tilde{P}_{ijI}^n = 0$ and $\tilde{P}_{ijII}^n = 0$. In addition, as $\theta = \pm\pi$ at the crack surfaces for a flat crack, ψ_{Ij} and ψ_{IIj} are functions only of ξ. The jump terms in the enriched DBIE remain the same as the jump terms arising from the strongly singular enriched integrals will cancel during implementation. The discretised TBIE is

$$n_i(\dot{x})\sum_{n=1}^{Ne}\sum_{a=1}^{M} E_{kij}^{na}u_k^{na} = n_i(\dot{x})\sum_{n=1}^{Ne}\sum_{a=1}^{M} F_{kij}^{na}t_k^{na} \tag{8}$$

where

$$E_{kij}^{na} = \int_{-1}^{1} N^a(\xi) S_{kij}(\grave{x}, x(\xi)) J^n(\xi) d\xi \qquad (9a)$$

$$F_{kij}^{na} = \int_{-1}^{1} N^a(\xi) D_{kij}(\grave{x}, x(\xi)) J^n(\xi) d\xi \qquad (9b)$$

Substituting the enriched form of displacement (5) into the integral equation (8) we arrive at

$$n_i(\grave{x}) \sum_{n=1}^{Ne} \sum_{a=1}^{M} E_{kij}^{na} u_k^{na} + n_i(\grave{x}) \sum_{a=1}^{Ne} \tilde{E}_{kijI}^{n} \tilde{K}_I$$

$$+ n_i(\grave{x}) \sum_{a=1}^{Ne} \tilde{E}_{kijII}^{n} \tilde{K}_{II} = n_i(\grave{x}) \sum_{n=1}^{Ne} \sum_{a=1}^{M} F_{kij}^{na} t_k^{na} \qquad (10)$$

where, if the element n is enriched,

$$\tilde{E}_{kijI}^{n} = \int_{-1}^{1} S_{kij}(\grave{x}, x(\xi)) \psi_{Ik}(\xi) J^n(\xi) d\xi \qquad (11a)$$

$$\tilde{E}_{kijII}^{n} = \int_{-1}^{1} S_{kij}(\grave{x}, x(\xi)) \psi_{IIk}(\xi) J^n(\xi) d\xi \qquad (11b)$$

or otherwise $\tilde{E}_{kijII}^{n} = 0$ and $\tilde{E}_{kijII}^{n} = 0$. Implementation of the TBIE and DBIE needs much care in evaluating the hyper-singular and strongly-singular integrals that arise (we note that the use of enrichment functions does not change the order of the singularity). However, useful techniques have been applied successfully to XBEM by Simpson [30], where the hyper-singular and strongly singular integrals have been evaluated using the Guiggiani method [34], and the Telles [35] adaptive method used for the weakly singular cases.

It is clear after introducing enrichment equations (6) and (10) that new degrees of freedom appear. The main advantage of formulating the enrichment as stated above is that the number of extra degrees of freedom is limited to two per crack tip. Thus, increasing the number of enriched elements has no effect on the size of the system. In order to achieve a square system of equations, an additional collocation point can be used, and this allows us to solve for $\tilde{K}_I$ and $\tilde{K}_{II}$ as part of the solution vector. Simpson and Trevelyan [30] suggest an alternative, generating additional equations in which the fundamental solution is replaced by pure mode I and mode II stress states. However, both methods were unable to evaluate accurate SIFs directly, and the J-integral was needed to find SIFs to the required accuracy.

3   Crack Tip Tying Constraint

In this section we introduce a new tying constraint that (i) provides a very simple form for the additional equations required to accommodate the extra

enrichment degrees of freedom, (ii) allows the enrichment amplitudes $\tilde{K}_I$ and $\tilde{K}_{II}$ to approximate closely the stress intensity factors K_I and K_{II}, and thereby (iii) removes the need for J-integral computations. This is achieved by the simple method of constraining against a displacement discontinuity at the crack tip.

We define as element A, parameterised by local variable ξ_A, the element on the upper crack surface and touching the crack tip at $\xi_A = 1$. We further define as element B, parameterised by local variable ξ_B, the element on the lower crack surface and touching the crack tip at $\xi_B = -1$. Applying the expression (5) to give the displacement at the crack tip which we denote point y, and equating the values from the elements A and B, we have

$$\tilde{K}_I\psi_{Ij}(y)+\tilde{K}_{II}\psi_{IIj}(y)+\sum_{a=1}^{M} N_A^a(1)u_{Aj}^a = \tilde{K}_I\psi_{Ij}(y)+\tilde{K}_{II}\psi_{IIj}(y)+\sum_{b=1}^{M} N_B^b(-1)u_{Bj}^b \tag{12}$$

Here $N_A^a(\xi_A)$ and $N_B^b(\xi_B)$ denote the shape functions for nodes a and b of elements A and B respectively. Terms u_{Aj}^a, u_{Bj}^b denote the coefficients multiplying the respective shape functions for these nodes (we are careful not to say they are nodal displacements, which they would be in conventional BEM, but are no longer because of the injection of the enrichment functions). Cancellation of the enrichment terms, which in any case vanish at the crack tip, the constraint becomes

$$\sum_{a=1}^{M} N_A^a(1)u_{Aj}^a = \sum_{b=1}^{M} N_B^b(-1)u_{Bj}^b \tag{13}$$

Using the constraint (13) for both x and y displacements provides two additional equations for each crack tip. These equations are appended to the BEM system formed by collocation at the nodes, creating a square system. Solution of the system allows $\tilde{K}_I$ and $\tilde{K}_{II}$ to be revealed in the solution column with remarkable accuracy.

4   Numerical Examples

4.1   Mode I

Two pure Mode I cases are selected to show the effect of crack tip displacement. The first case (**case 1**) is a centre crack in an infinite homogeneous elastic flat plate as shown in Figure 2. This has a well-known exact solution in which the crack tip displacement is zero. The XBEM model is formed from the actual crack surfaces along with a contour, Γ_{ext}, truncating the infinite domain. This contour is formed so that the entire XBEM domain lies close to the crack tip and so pure mode I applies. Traction-free crack surfaces are prescribed, and on Γ_{ext} displacements calculated by Williams expansions have been used as boundary conditions. The second case (**case 2**) considers an edge crack in a flat plate under uniaxial traction (pull-pull) as shown in Figure 3. The reference solution [36] represented by a ratio of K_I/K_0 has been used as there is no exact solution
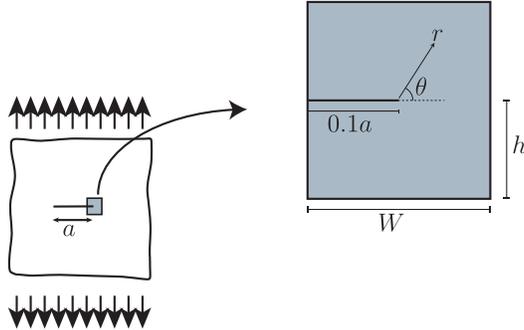
Figure 2: Infinite flat plate (case 1)
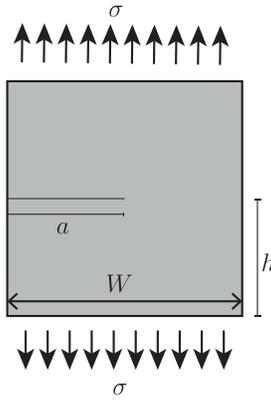
Figure 3: Square flate plate under axial tension (case 2)

available. The considered dimensions are $a = h = 0.5W$. Both cases are treated as plane stress.

case 1 : Figure 4 shows the displaced shape considering (a) the component of the displacement for the crack surface enriched elements associated with the first and the second term of Eq.(5); (b) the component of the displacement represented by the shape function expansion in the last term of Equation (5), and (c) the total displacement considering all three terms of (5). In this special case the enrichment functions ψ_{Ij}, ψ_{IIj} are capable of capturing the displacement field over the crack surfaces. As a result there is no contribution from the shape functions. In Figure 6a we display the percentage errors in the SIF K_I using (i) conventional, unenriched DBEM with the J-integral, (ii) enriched XBEM with the J-integral, (iii) direct $\tilde{K}_I$ from enriched XBEM using extra collocation points to provide the additional integral equations required, and (iv) direct $\tilde{K}_I$ from enriched XBEM using Equation (13) to enforce displacement continuity at the crack tip. It is seen that all the enriched methods produce highly accurate SIF results in comparison with the conventional (piecewise polynomial)

9
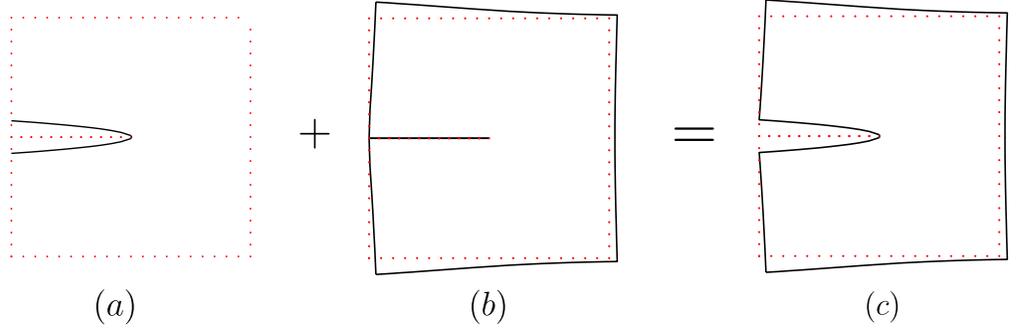
Figure 4: Displacment components for case 1
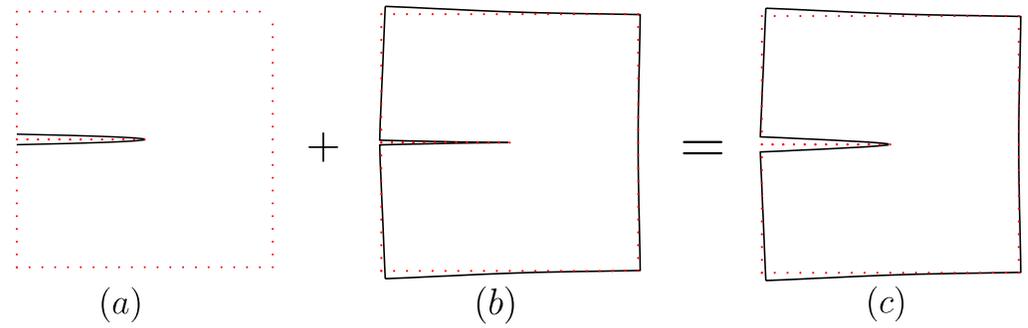
Figure 5: Displacment components for case 2
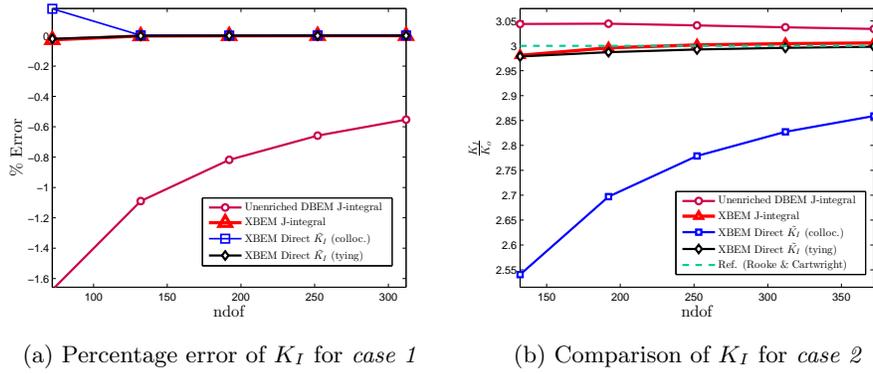
(a) Percentage error of K_I for *case 1*

(b) Comparison of K_I for *case 2*

Figure 6: Results of K_I for Mode I using various methods

10

Table 1: Errors comparison for case 1

Method	ndof	K_I	% Error
Unenriched DBEM J-integral	312	17626523.75	-0.55299
XBEM J-integral	314	17724524.44	-0.00008
XBEM Direct $\tilde{K}_I$ (colloc.)	314	17724790.96	0.00142
XBEM Direct $\tilde{K}_I$ (Tying)	314	17724564.26	0.000145

Table 2: case 2 results compared to [36]

Method	ndof	K_I	$\frac{K_I}{K_o}$
Unenriched DBEM J-integral	372	53775818.85	3.034
XBEM J-integral	374	53299223.93	3.007
XBEM Direct $\tilde{K}_I$ (colloc.)	374	50677080.10	2.859
XBEM Direct $\tilde{K}_I$ (Tying)	374	53142056.71	2.998

BEM J-integral solutions. Because the enrichment is ideal, these results can be achieved with very small numbers of degrees of freedom. In order to make a comparison of the accuracy of the different methods, we focus on the set of results at 312 and 314 degrees of freedom from Fig. 6a. Table 1 shows the error compared to exact KI, which can be calculated as $17.7245 MPa\sqrt{m}$.

case 2 : The displaced shape for the second case is presented in Figure 5, which shows the displacement component represented by the first and the second terms of Eq.(5), Fig. 5b the displacement contribution by shape function terms in (5), and Figure 5c which shows the total displacement considering all three terms of (5). It is evident that the enrichment functions no longer provide a complete basis for the crack displacement, and the shape functions are required to compensate, so that the total displacement is approximated accurately. Figure 6b shows the convergence of the various methods we test (note that the reference solution is approximate). In Table 2 we present the numerical values of K_I/K_o, for the models having 372 and 374 degrees of freedom. It can be seen that the XBEM with J-integral and the direct method using the tying constraint are both capable of delivering results very close to the reference solution.

Comparing the directly computed $\tilde{K}_I$ from enriched XBEM using extra collocation points in **case 1** and **2** shows the effect of the displacement discontinuity at the crack tip. It is immediately evident that the use of the XBEM enrichment (5) without the use of the constraint (13) causes a significant deterioration in the ability of $\tilde{K}_I$ to approximate K_I directly, and that in this case a J-integral is necessary. The injection of the tying constraint, forcing displacement continuity at the crack tip, allows the directly calculated $\tilde{K}_I$ to approximate K_I well. Remarkable results have been achieved which show better accuracy compared to conventional J-integral BEM approaches.
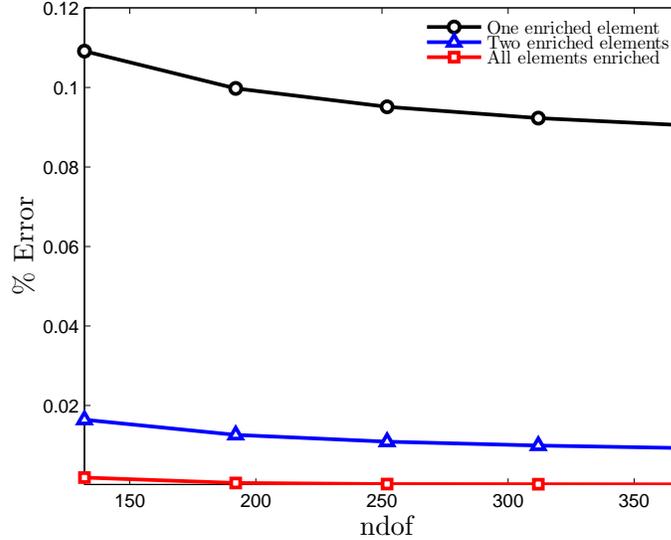
Figure 7: Effect of the number of enriched elements (case 1)

4.1.1 Number of enriched elements

A useful feature of the new enrichment presented in this paper is that the enrichment functions are not associated with nodal degrees of freedom as in the Partition of Unity Method. Instead, since the new degrees of freedom $\tilde{K}_I, \tilde{K}_{II}$ are associated with the crack tip, this enrichment technique gives us the freedom to increase the number of enriched elements without increasing the DOFs. The enrichment degrees of freedom are limited to two per crack tip. By the term "enriched element" we describe an element (on a crack surface) over which the displacement is approximated by equation (5). The number of enriched elements has a significant effect on the results, both when the J-integral is used to determine the SIFs and when the directly calculated $\tilde{K}_I, \tilde{K}_{II}$ are used. For example, Figure 7 shows the reduction in error for **case 1** when all crack surface elements are enriched. For this reason, all results in this paper are presented for models in which all elements on crack surfaces are enriched.

4.1.2 Order of extrapolation for tying constraint

The tying constraint enforces continuity of displacement at the crack tip, expressed through the equality of the displacements at this point as found by extrapolation of displacements over the upper and lower crack surfaces. The constraint is presented in Equation (13) by basing the extrapolation on the M nodes of each element touching the crack tip. We use three-noded, quadratic discontinuous elements (i.e. $M = 3$). However, it is possible to use a higher

12
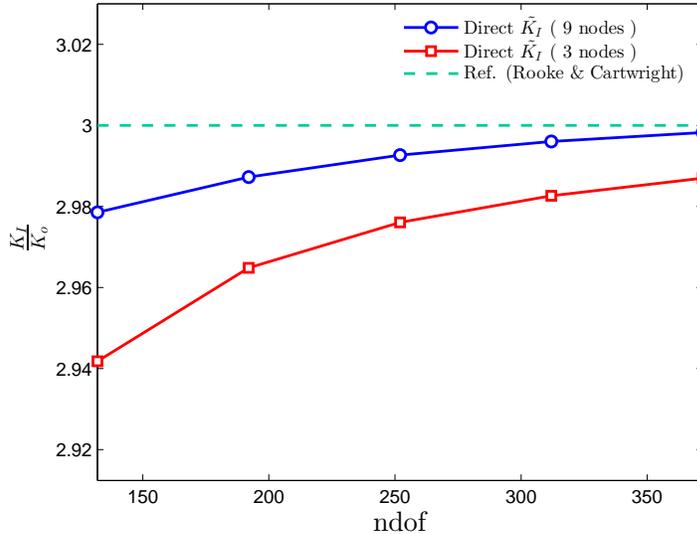
Figure 8: Effect of order of displacement extrapolation (case 2)

order Lagrangian extrapolation by considering the nodes on more elements.

This technique has been found to give improved accuracy. Figure 8 shows a comparison made (for the problem **case 2**) of the convergence of SIF results obtained through different orders of extrapolation. We compare results using 3 nodes to extrapolate displacement to those when 9 nodes are used. These are the nearest nine nodes to the crack tip on each crack surface. An improvement can be seen as a result of increasing the order used for extrapolation of displacement results to the crack tip. It is tempting to suggest using even higher order Lagrangian polynomials; however, this can increase error due to Rung's phenomenon.

4.2   Pure Mode II

We consider a square domain surrounding the tip of a crack in pure mode II. The problem is shown in Figure 9; dimensions used in the analysis are $h = a = 0.5W$. We prescribe boundary conditions as follows: The elements on the two crack faces are traction-free, and to the elements on all other parts of the square boundary of the domain we apply a displacement boundary condition equal to the pure mode II case. We use the algorithm described in the paper to determine K_{II}, the exact solution for which is $K_{II} = \sigma\sqrt{\pi a}$, and compare the errors in the term $\tilde{K}_{II}$ against those from both a conventional BEM solution and an enriched XBEM solution, both using the J-integral. This comparison is shown in Figure 10 and shows both enriched methods to provide highly accurate solutions in comparison to the more slowly converging results of the classical DBEM. As for

13
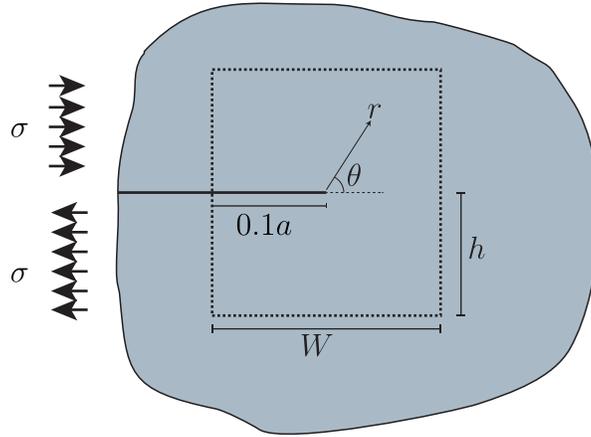
Figure 9: A square section sheet subject to shear

the case 1 considered in the mode I experiments, the enrichment is ideal here leading to very small errors. To clarify further, the exact behaviour is included in the approximation space through (in the mode II case) the second term on the right hand side of equation (5). The role of the last term in (5) can be viewed as the use of piecewise polynomials to capture the difference between pure mode I and II and the displacements in the case under analysis. Cases in which the enrichment is not ideal, i.e. we are not considering pure mode I and II, are considered in the following sections.

4.3   Bending

A rectangular plate under bending is considered as shown in Fig. 11. The plate is subjected to a bending moment applied to the upper and lower surfaces, as shown in the figure, and we consider the case $b = 2a$. We compare the convergence of the two enriched formulations and classical unenriched DBEM in terms of the normalised stress intensity factor K_I/K_o (where $K_o = 6M\sqrt{\pi a}/b^2$). The comparison is presented in Figure 12, and shows smooth convergence toward the reference value from [36](we note the reference solution is presented in [36] with accuracy of 1% which is rather large in comparison with the errors we are finding).

4.4   Mixed Mode

In this section we apply the proposed enrichment to a mixed mode case of an inclined edge crack in a finite plate under uniaxial tensile load. For mixed mode cases it is customary to use a decomposition technique [37] when using the J-integral in order to solve for both K_I and K_{II}. The plate contains an edge inclined crack at an angle β as shown in Figure 13. The problem does not have exact solution; instead, the numerical solution obtained by Xiao et al. [7] is

14
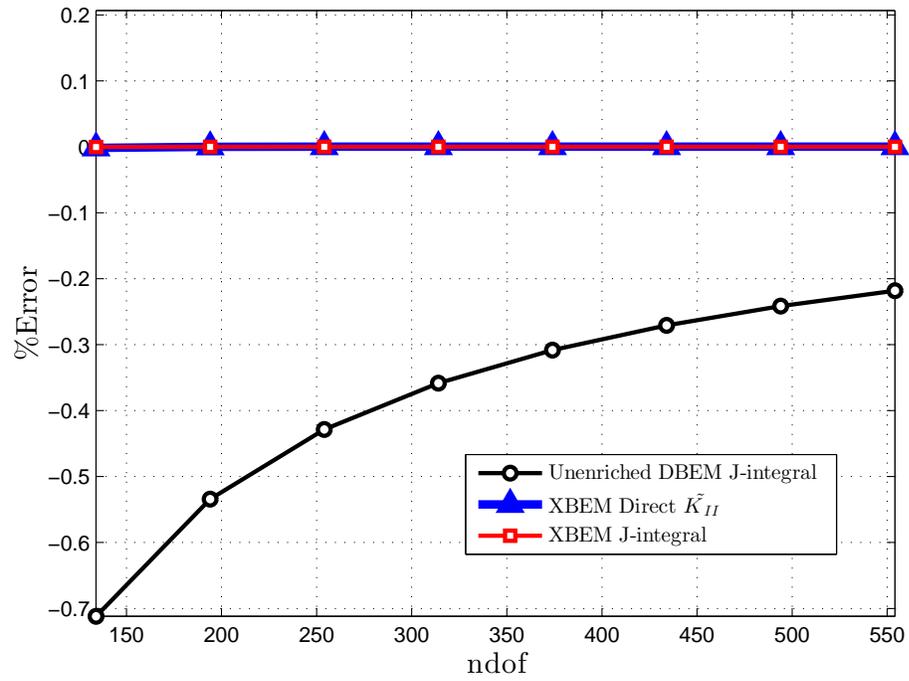
Figure 10: Results for pure Mode II
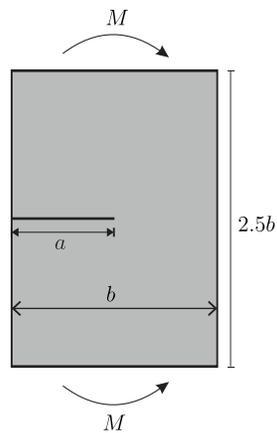
Figure 11: Rectangular plate under bending
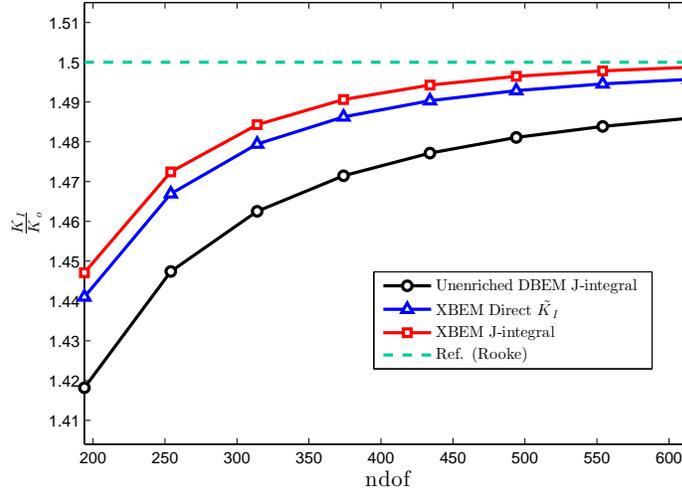
Figure 12: A comparison of normalised results for bending plate

used. The plate dimensions are $W = h = 1$, $a = 0.6$ and the angle of inclination β is 30°. We consider Young's modulus and Poisson's ratio to be 10^5 and 0.25 respectively. Uniaxial tension $\sigma = 1$ is applied over the top edge of the plate, and zero displacement prescribed in both directions at the lower end.

Results for K_I and K_{II} are presented in Figures 14 and 15; the same methods as above have been used to evaluate the SIFs at various model sizes. The reference solution is plotted as a horizontal line for comparison; the reader is reminded that this is also a numerical approximation and included for purposes of comparison. In the results it can be seen that the direct method is smoothly converging toward the same value as the J-integral methods.
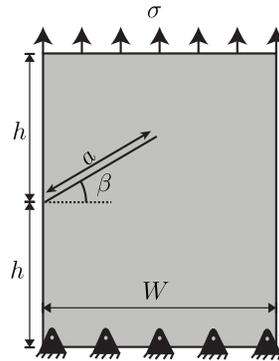
Figure 13: Rectangular plate subject to shear [16]
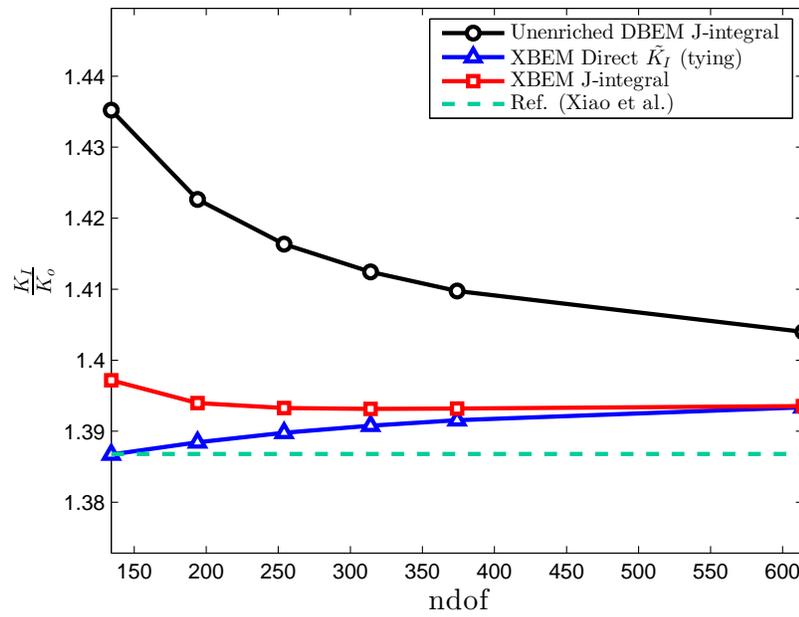
Figure 14: K_I for inclined crack results compared to Xiao et al. [7]
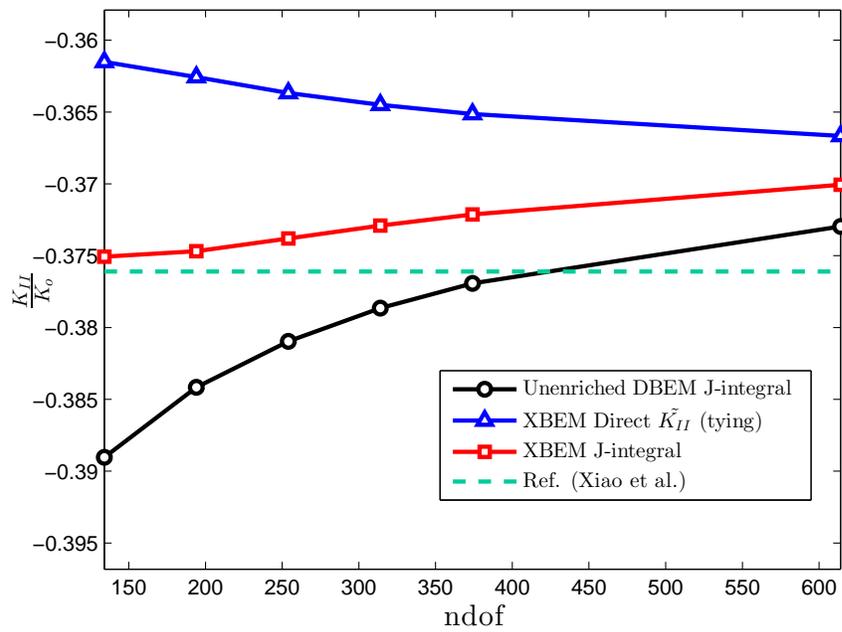
Figure 15: K_{II} for inclined crack results compared to Xiao et al. [7]

5   Conclusion

A new, extended dual boundary element method has been presented in which the enrichment functions are based closely on the stress intensity factors in Linear Elastic Fracture Mechanics theory for 2D. The enrichment adds only two degrees of freedom per crack tip. The extra equations that are therefore required are derived from enforcement of displacement continuity at the crack tip. The method is able to evaluate SIFs directly without any requirement for postprocessing calculations such as the J-integral. Results are improved by increasing the number of enriched elements. Since this can be done without increasing the size of the system, and with negligible extra computational cost, the optimum is to enrich all crack surface elements for more accuracy. Further accuracy can be obtained by using high (8th) order Lagrangian polynomials in applying the crack tip tying constraint. Strongly singular and hypersingular integrals that arise, can be evaluated using Guiggiani method [34] as illustrated in [29, 30]. The SIFs found from the direct method converge to the same values as those from the J-integral, and the method clearly outperforms the use of the piecewise polynomial dual BEM. Results are shown for two mode I problems and a mixed mode problem.

Current work by the authors involves extending these ideas to 3D, where it is expected that the ability to produce accurate SIFs without recourse to the J-integral will be of significant benefit.

Acknowledgement

References

[1] William, M.L.. On the stress distribution at the base of a stationary crack. J Applied Mechanic 1957;24:109–11.

[2] Tada, H., Paris, P.C., Irwin, G.R.. The Stress Analysis of Cracks - Handbook. Paris Productions Inc., St Louis, MO; 1985.

[3] Jr, V.. The finite element method for prediction of crack behavior. Nuclear Engineering and Design 1970;11(2):323 – 332.

[4] Benzley, S.E.. Representation of singularities with isoparametric finite elements. International Journal for Numerical Methods in Engineering 1974;8:537–545.

[5] Henshell, R.D., Shaw, K.G.. Crack tip finite elements are unnecessary. International Journal for Numerical Methods in Engineering 1975;9:495–507.

[6] Tong, P., Pian, T.H., Lasry, S.J.. A hybrid-element approach to crack problems in plane elasticity. International Journal for Numerical Methods in Engineering 1973;7:297–308.

[7] Xiao, Q.Z., Karihaloo, B.L., Liu, X.Y.. Direct determination of sif and higher order terms of mixed mode cracks by a hybrid crack element. International Journal of Fracture 2004;125(3-4):207–225.

[8] Leung, A., Su, R.. Mode I crack problems by fractal two level finite element methods. Engineering Fracture Mechanics 1994;48:847 – 856.

[9] Leung, A., Su, R.. Mixed-mode two-dimensional crack problem by fractal two level finite element method. Engineering Fracture Mechanics 1995;51:889 – 895.

[10] Su, R., Sun, H., Leung, A.. Determination of crack tip asymptotic stress field by fractal finite element method. In: Computational Fluid and Solid Mechanics 2003. Oxford: Elsevier Science Ltd. ISBN 978-0-08-044046-0; 2003, p. 662 – 665.

[11] Su, R., Fok, S.. Determination of coefficients of the crack tip asymptotic field by fractal hybrid finite elements. Engineering Fracture Mechanics 2007;74:1649 – 1664.

[12] Treifi, M., Oyadiji, S.O.. Evaluation of mode III stress intensity factors for bi-material notched bodies using the fractal-like finite element method. Computers & Structures 2013;129:99 – 110.

[13] Chidgzey, S.R., Deeks, A.J.. Determination of coefficients of crack tip asymptotic fields using the scaled boundary finite element method. Engineering Fracture Mechanics 2005;72(13):2019 – 2036.

[14] Bird, G.E., Trevelyan, J., Augarde, C.E.. A coupled bem/scaled boundary FEM formulation for accurate computations in linear elastic fracture mechanics. Engineering Analysis with Boundary Elements 2010;34:599 – 610.

[15] Melenk, J., Babuška, I.. The partition of unity finite element method: Basic theory and applications. Computer Methods in Applied Mechanics and Engineering 1996;139:289 – 314.

[16] Belytschko, T., Black, T.. Elastic crack growth in finite elements with minimal remeshing. International Journal of Fracture Mechanics 1999;45:601–620.

[17] Cruse, T.A.. Numerical evaluation of elastic stress intensity factors by the boundary-integral equation method. The surface Crack: Physical and Computational Solutions 1972;:153–170.

[18] Snyder, M., Cruse, T.. Boundary-integral equation analysis of cracked anisotropic plates. International Journal of Fracture 1975;11(2):315–328.

[19] Blandford, G.E., Ingraffea, A.R., Liggett, J.A.. Two-dimensional stress intensity factor computations using the boundary element method. International Journal for Numerical Methods in Engineering 1981;17(3):387–404.

[20] Hong, H., Chen, J.. Derivations of integral equations of elasticity. J Eng Mech 1988;114:1028–1044.

[21] HONG, H.K., Chen, J.T.. Generality and special cases of dual integral equations of elasticity. Chinese Society of Mechanical Engineers, Journal 1988;9:1–9.

[22] Chen, J., Hong, H.K.. Singularity in darcy flow around a cutoff wall. Advances in Boundary Elements: Field and Fluid Flow Solution 1989;2:15–27.

[23] Portela, A., Aliabadi, M.H., Rooke, D.P.. The dual boundary element method: Effective implementation for crack problems. International Journal for Numerical Methods in Engineering 1992;33:1269–1287.

[24] Chen, J.T., Hong, H.K.. Review of dual boundary element methods with emphasis on hypersingular integrals and divergent series. Applied Mechanics Reviews 1999;52:17–33.

[25] Mi, Y., Aliabadi, M.. Dual boundary element method for three-dimensional fracture mechanics analysis. Engineering Analysis with Boundary Elements 1992;10(2):161–171.

[26] Marburg, S.. Discretization requirements: How many elements per wavelength are necessary? In: Computational Acoustics of Noise Propagation in Fluids-Finite and Boundary Element Methods. Springer; 2008, p. 309–332.

[27] Garcıa, F., Sáez, A., Domınguez, J.. Traction boundary elements for cracks in anisotropic solids. Engineering analysis with boundary elements 2004;28(6):667–676.

[28] Portela, A., Aliabadi, M.H., Rooke, D.P.. Efficient boundary element analysis of sharp notched plates. International Journal for Numerical Methods in Engineering 1991;32:445–470.

[29] Simpson, R., Trevelyan, J.. A partition of unity enriched dual boundary element method for accurate computations in fracture mechanics. Computer Methods in Applied Mechanics and Engineering 2011;200(1 - 4):1 – 10.

[30] Simpson, R., Trevelyan, J.. Evaluation of J_1 and J_2 integrals for curved cracks using an enriched boundary element method. Engineering Fracture Mechanics 2011;78(4):623–637.

[31] Rice, J.R.. A path independent integral and approximate analysis of strain concentraion by notches and cracks. Journal of Applied Mechanics 1968;35:379–386.

[32] Helsing, J.. Fast and accurate numerical solution to an elastostatic problem involving ten thousand randomly oriented cracks. International Journal of Fracture 2000;100(4):321–327.

[33] Li, S., Mear, M., Xiao, L.. Symmetric weak-form integral equation method for three-dimensional fracture analysis. Computer Methods in Applied Mechanics and Engineering 1998;151(3):435–459.

[34] Guiggiani, M., Krishnasamy, G., Rudolphi, T.J., Rizzo, F.J.. A general algorithm for the numerical solution of hypersingular boundary integral equations. ASME Jornal of Applied Mechanics 1992;59:604–614.

[35] Telles, J.C.F.. A self-adaptive co-ordinate transformation for efficient numerical evaluation of general boundary integrals. International Journal for Numerical Methods in Engineering 1987;24:959 – 973.

[36] Rooke, D.P., Cartwright, D.J.. Compendium of Stress Intensity Factors. Stationery Office, Great Britain, Ministry of Defence, Procurement Executive; 1976.

[37] Aliabadi, M.H.. Evaluation of mixed mode stress intensity factors using path independent integral. In: Proceedings of the 12th International Conference on Boundary Element Methods. Computational Mechanics Publications; 1990, p. 281–292.